Electronic Supplementary Material (ESI) for Energy & Environmental Science.
This journal is © The Royal Society of Chemistry 2022

Supplementary information

A tailored electrolyte for safe and durable potassium ion batteries

Ling Fan[1†]*, Huabin Xie[1†], Yanyao Hu[1], Zhuoma Caixiang[1], Apparao M. Rao[2], Jiang Zhou[3], Bingan Lu[1]*

[1]School of Physics and Electronics, Hunan University, Changsha, 410083, P. R. China.

[2]Department of Physics and Astronomy, Clemson Nanomaterials Institute, Clemson University, Clemson, SC, USA.

[3]School of Materials Science and Engineering, Central South University, Changsha, 410083, P. R. China.

[†]These authors contributed equally to this work.

*Corresponding author. Email: fanling@hnu.edu.cn (L. Fan); luba2012@hnu.edu.cn (B. Lu)

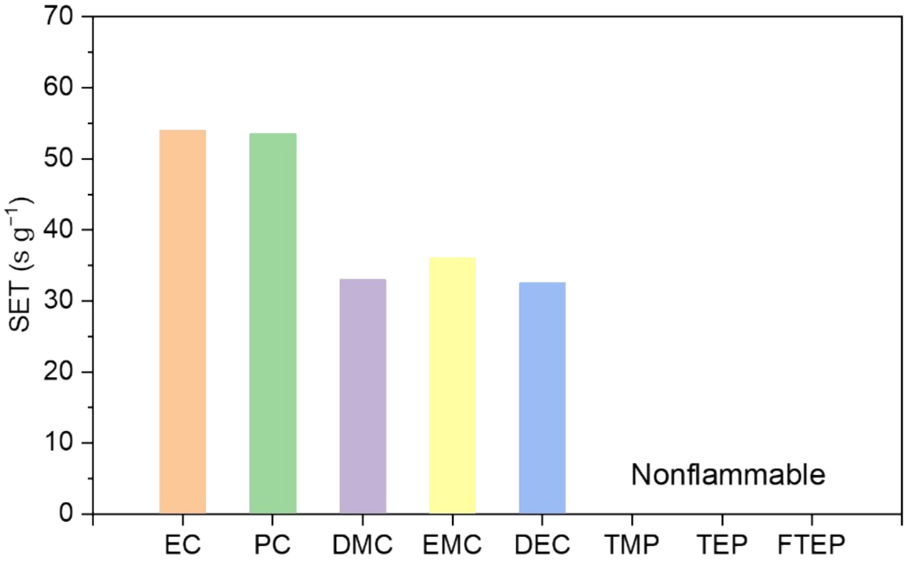

Fig. S1. The self-extinguishing time (SET) of the electrolytes with 1 M KFSI in various solvents.

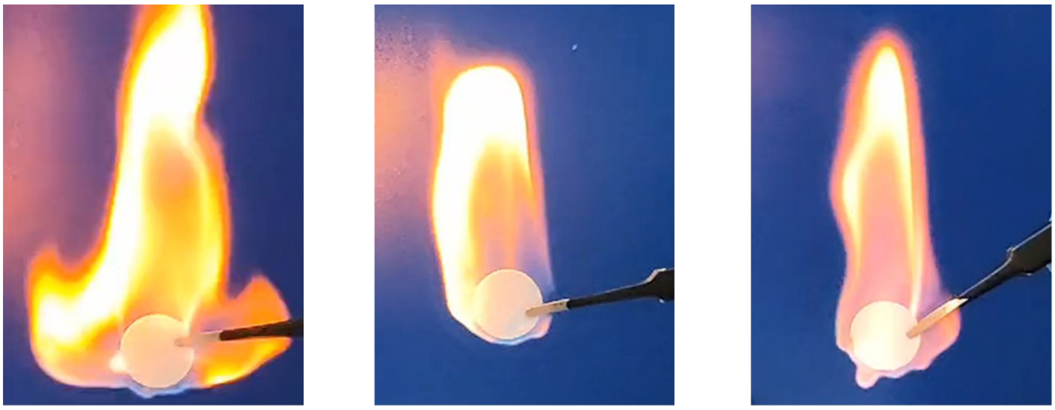

3 M KFSI-DME　　0.8 M KPF_6-EC:DEC　　0.8 M KFSI-EC:DEC

Fig. S2. The flame tests of a highly concentrated electrolyte and the commonly used potassium ion electrolytes.

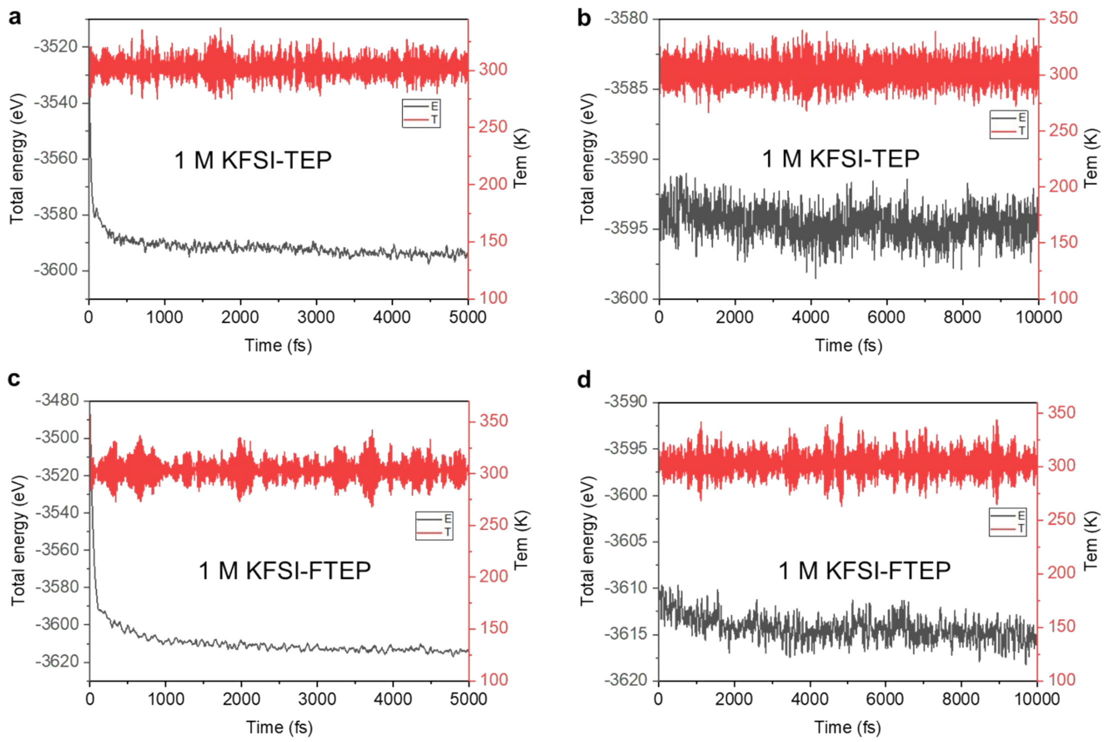

Fig. 3. Fluctuations of total energy and temperature of the electrolytes during simulations. (**a**) The 5 ps pre-equilibrium process and (**b**) the 10 ps production process of 1 M KFSI-TEP electrolyte. (**c**) The 5 ps pre-equilibrium process and (**d**) the 10 ps production process of 1 M KFSI-FTEP electrolyte.

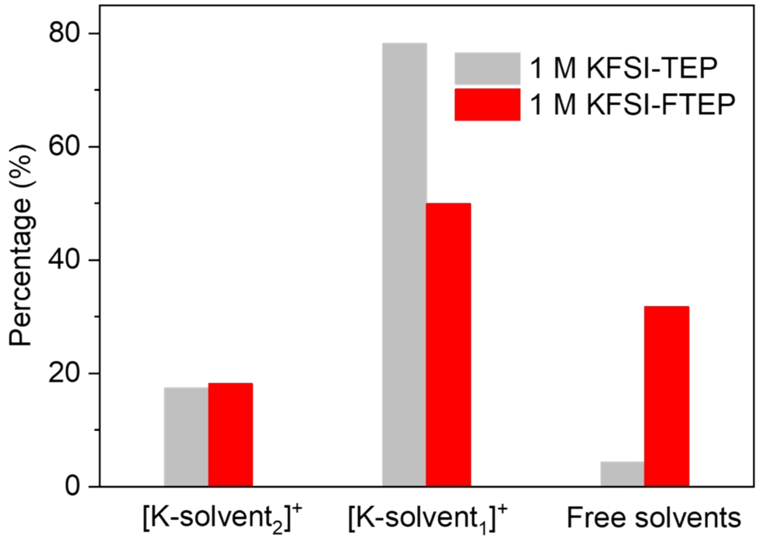

Fig. S4. The percentage of solvents coordinated to K^+ in the two electrolytes.

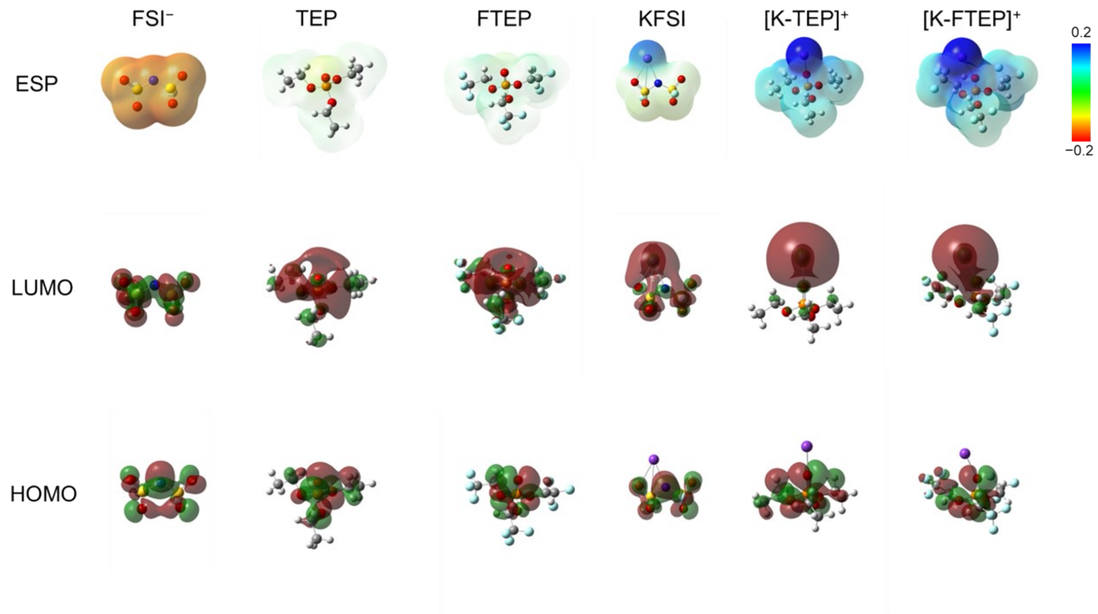

Fig. S5. The LUMO-HOMO energy levels and the electrostatic potential (ESP) maps of various molecules and complexes.

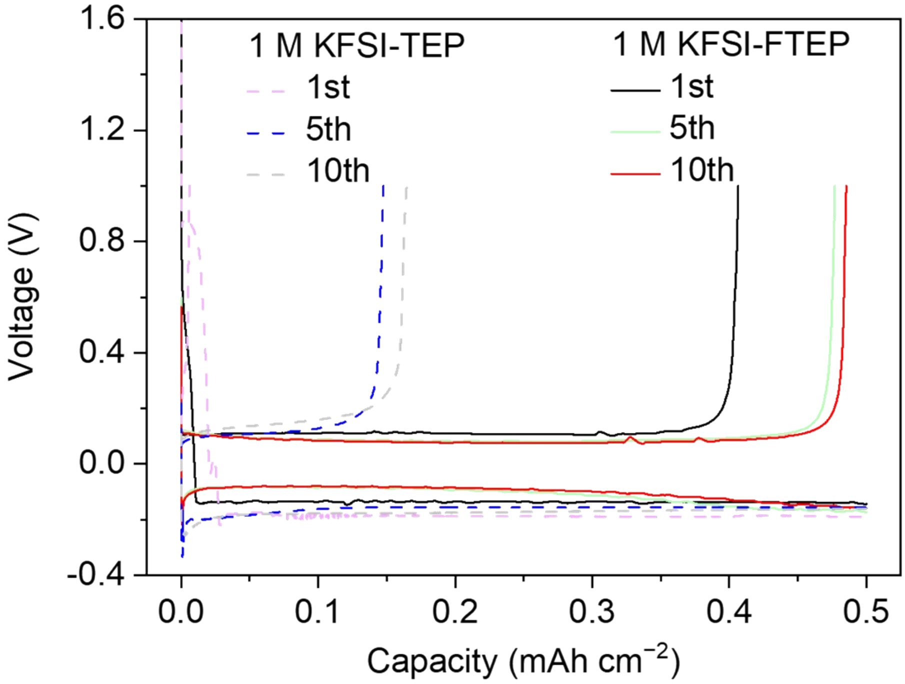

Fig. S6. The plating/stripping profiles of K||Cu cells with an areal capacity of 0.5 mAh cm^{-2} under 0.1 mA cm^{-2}.

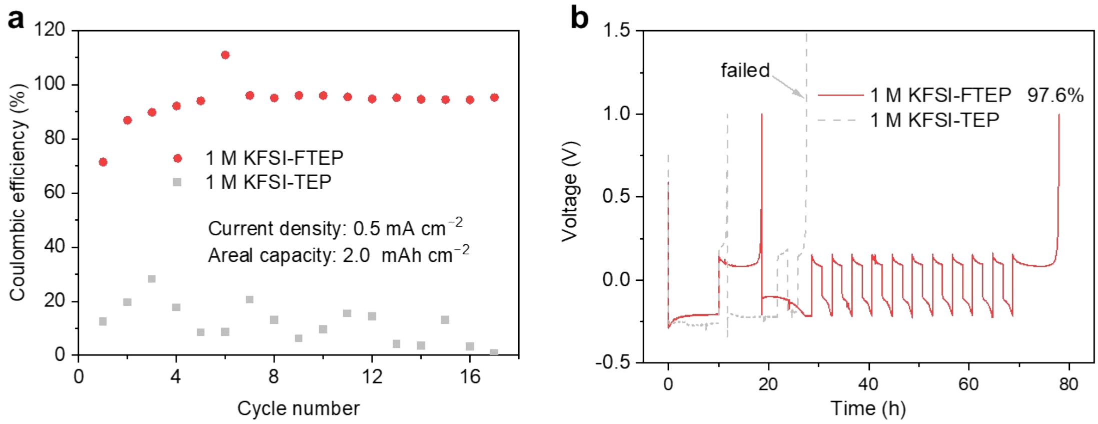

Fig. S7. (**a**) The cycling performance of the K||Cu cells with different electrolytes at a current density of 0.5 mA cm^{-2} and areal capacity of 2 mAh cm^{-2}. (**b**) The Aurbach efficiency of K||Cu cells with different electrolytes.

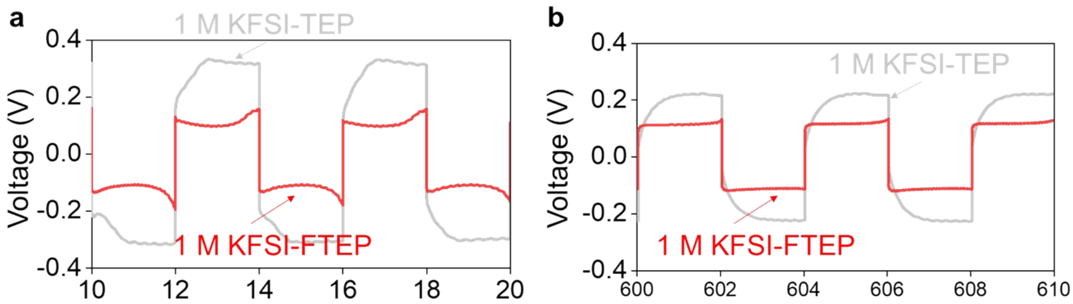

Fig. S8. The K plating/stripping voltage profiles of K||K symmetric cells with the two electrolytes.

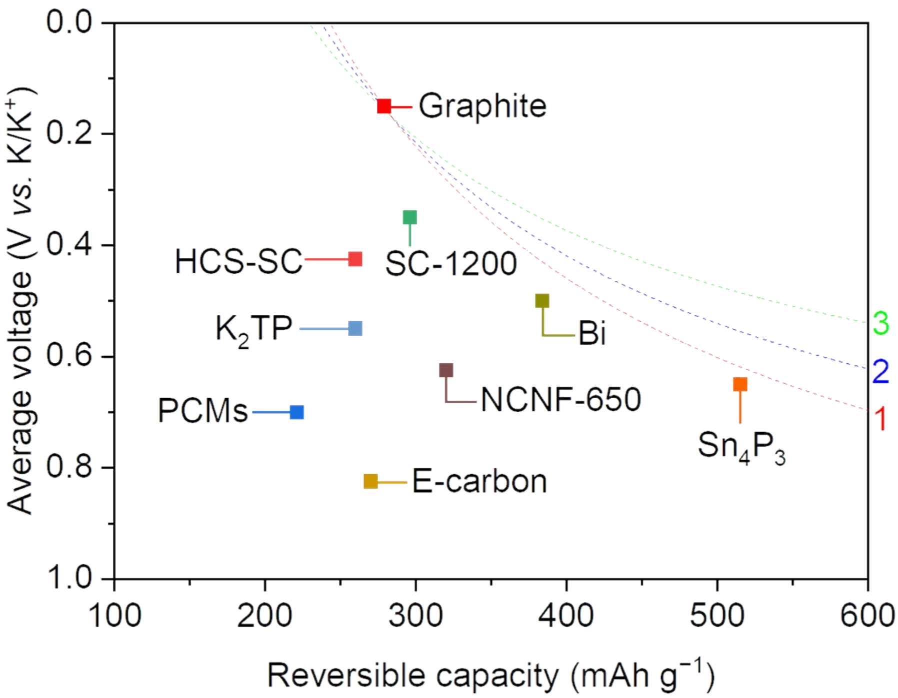

Fig. S9. The summarized capacity–voltage plots of different anode materials[37-43, 46]. Note: The dotted lines 1, 2, and 3 represent the isoenergy density curve of the required average voltage and capacity of an anode to achieve the energy density of graphite (capacity of 279 mAh g^{-1} and average voltage of 0.15 V). The isoenergy density curve is calculated as reported in previous literature[7]. Dotted line 1: Coupled with $KVOPO_4$ cathode[44] (capacity of 115 mAh g^{-1} and average voltage of 3.65 V). Dotted line 2: Coupled with $K_{0.5}MnO_2$ cathode[45] (capacity of 127 mAh g^{-1} and average voltage of 2.95 V). Dotted line 3: Coupled with PTCDA cathode[10] (capacity of 131 mAh g^{-1} and average voltage of 2.4 V). When coupled with the above cathodes to assemble full cells, the energy density of a full cell with graphite as the anode is higher than that with most reported anode materials.

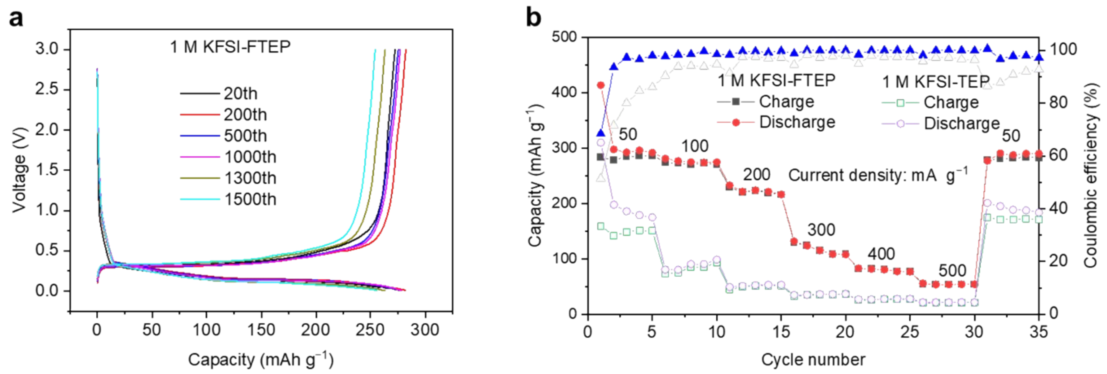

Fig. S10. (**a**) The charge-discharge profiles of graphite electrode with 1 M KFSI-FTEP as the electrolyte. (**b**) The rate performance of the graphite electrode with the two electrolytes.

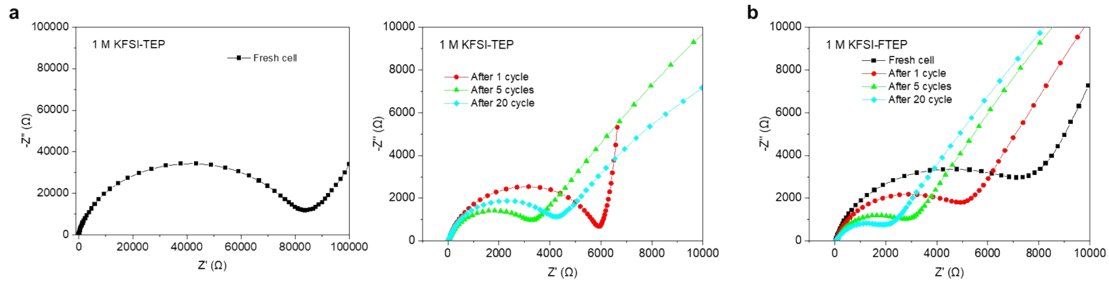

Fig. S11. The electrochemical impedance spectroscopy (EIS) of graphite electrodes with the two electrolytes. (**a**) In 1 M KFSI-TEP electrolyte. (**b**) In 1 M KFSI-FTEP electrolyte.

Clearly, the overall interfacial resistance of K||graphite cells in 1 M KFSI-TEP electrolyte are firstly shifts to lower values (from the fresh cell to the 5th cycles), and then it was increased from the 5th cycles to 20th cycles. The decreased interfacial resistance is likely because of the activation and the SEI formation process during the initial cycles, while the increase of interfacial resistance after 20 cycles is might be due to the continuously decomposition of electrolyte and formation of thick SEI, which is detrimental to its electrochemical performance. In contrast, the overall interfacial resistance of K||graphite cells in 1 M KFSI-FTEP electrolyte are continuously shifts to lower values with cycles, possibly caused by a more favorable activation process, and the low interfacial resistance is conducive to achieving excellent electrochemical performance.

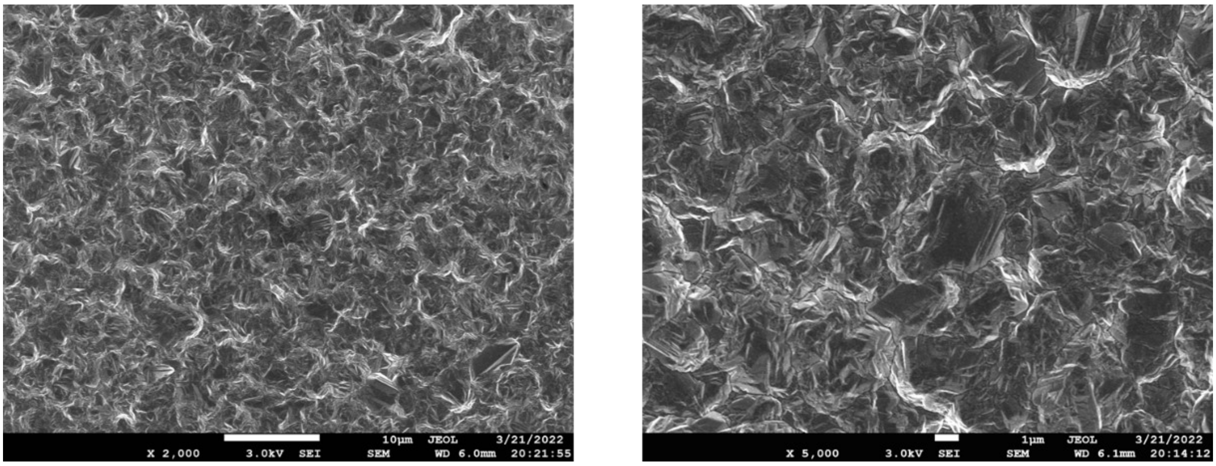

Fig. S12. The SEM image of bare Cu foil.

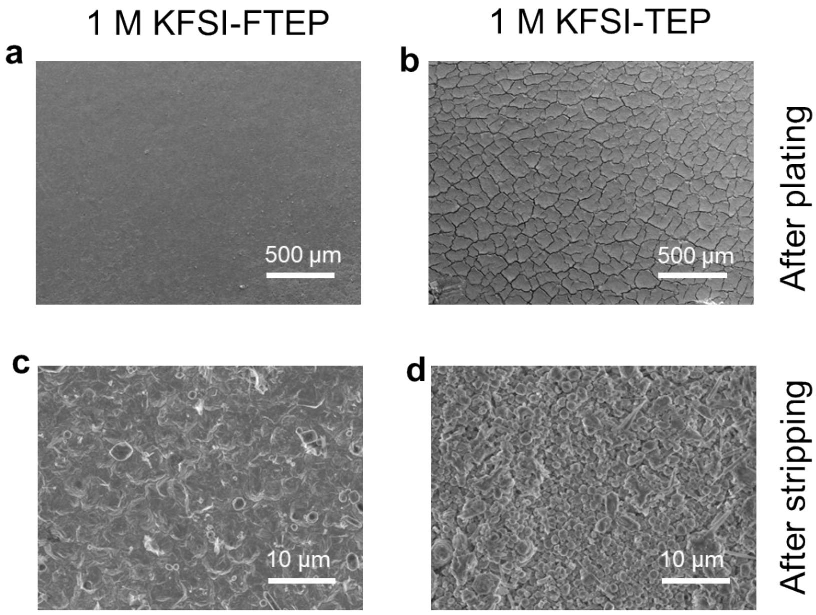

Fig. S13. The SEM images of Cu foil after plating or stripping with the two electrolytes. (**a** and **b**) After plating. (**c** and **d**) After stripping. (**a** and **c**) 1 M KFSI-FTEP electrolyte. (**b** and **d**) 1 M KFSI-TEP electrolyte.

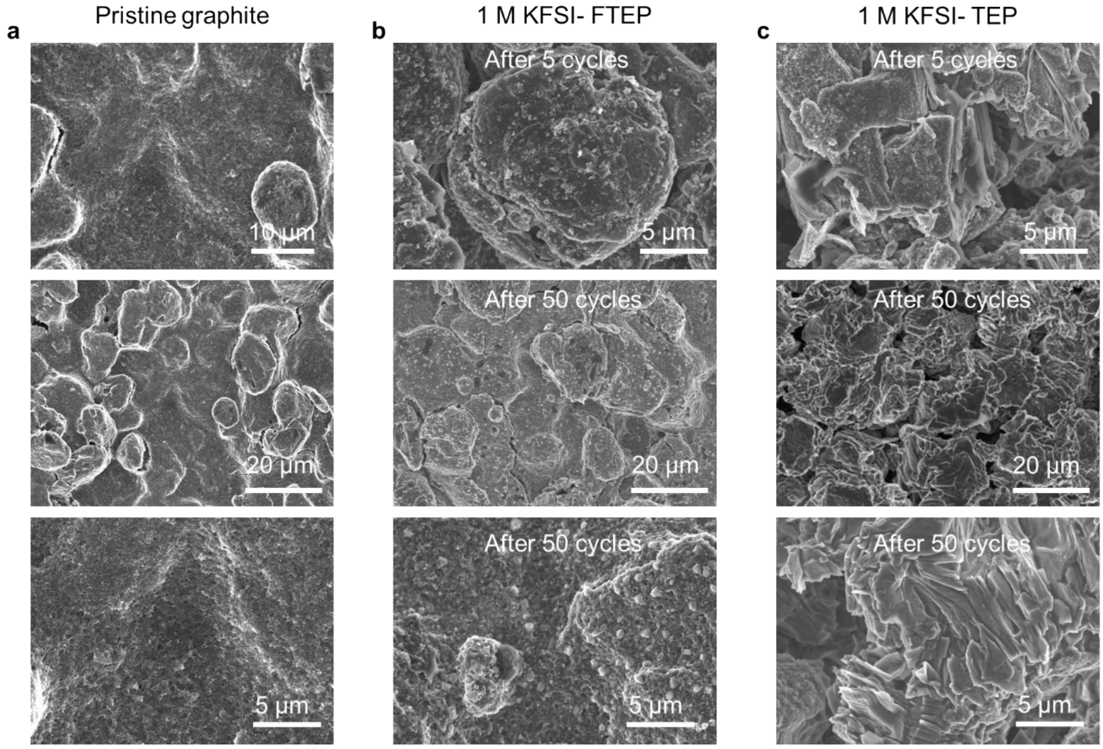

Fig. S14. The SEM images of graphite electrodes before and after different cycles with the two electrolytes. (**a**) Pristine graphite. (**b**) Graphite electrode after different cycles with 1 M KFSI-FTEP electrolyte. (**c**) Graphite electrode after different cycles with 1 M KFSI-TEP electrolyte.

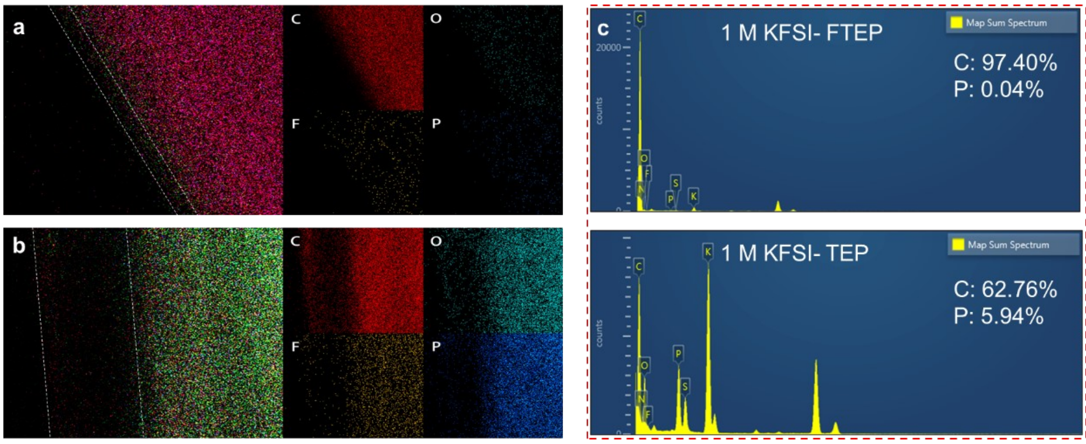

Fig. S15. Elemental mappings and elemental counts of graphite electrodes after 5 cycles with the two electrolytes. (**a**) 1 M KFSI- FTEP electrolyte. (**b**) 1 M KFSI- TEP electrolyte. (**c**) Elemental counts of graphite electrodes with two electrolytes.

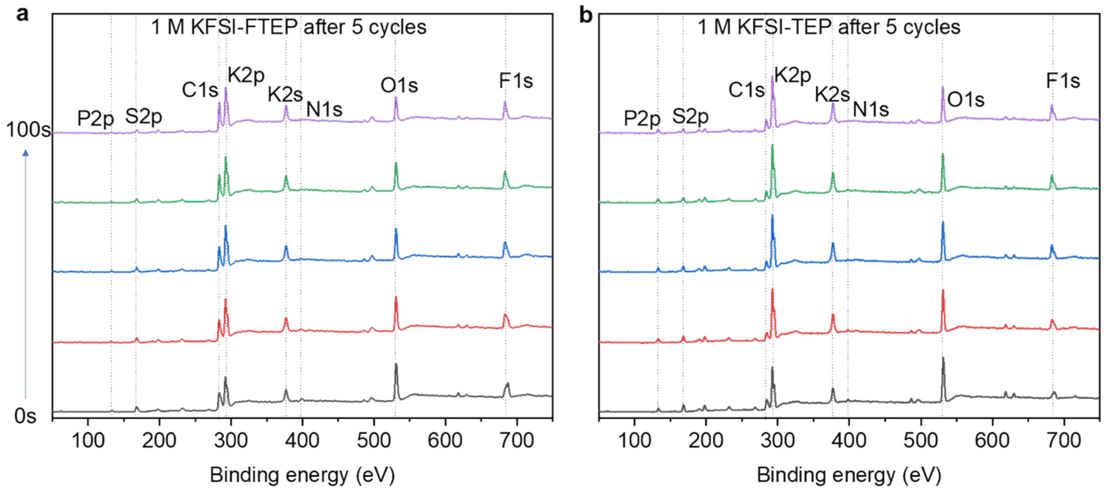

Fig. S16. The full survey XPS of the graphite electrode after 5 cycles with the two electrolytes. (**a**) 1 M KFSI- FTEP electrolyte. (**b**) 1 M KFSI- TEP electrolyte.

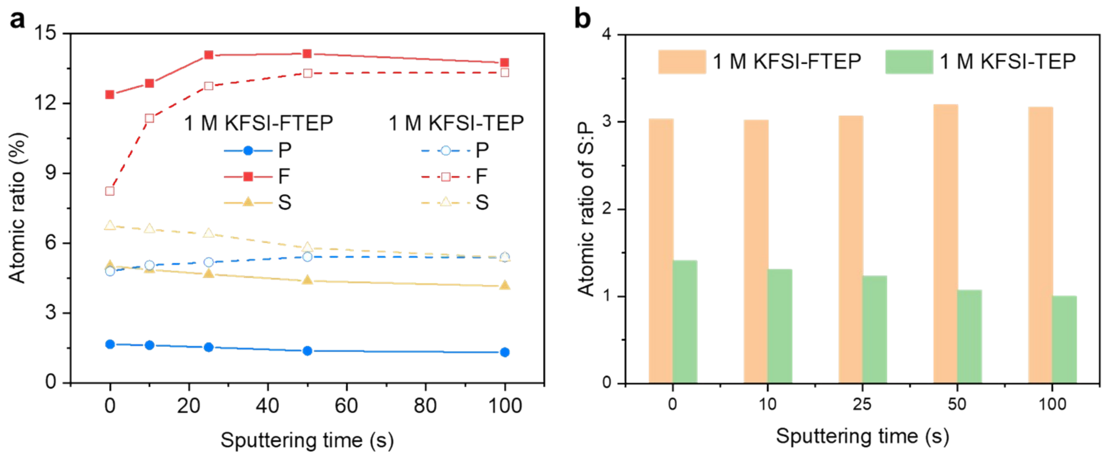

Fig. S17. (**a**) The atomic ratios of P, F, and S elementals on graphite electrodes at different depths after 5 cycles. (**b**) The atomic ratios of S:P on graphite electrodes at different depths after 5 cycles.

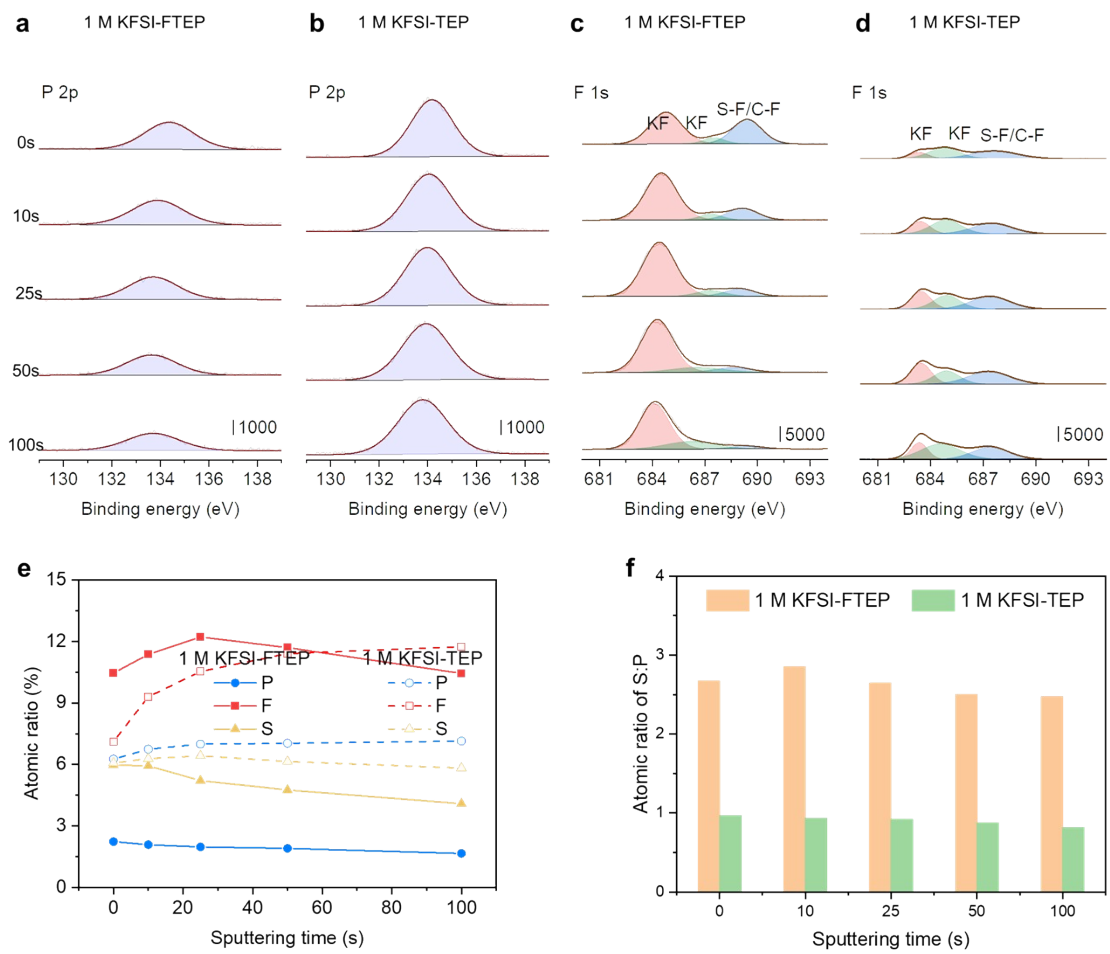

Fig. S18. The XPS characterizations of the graphite electrode after 50 cycles with the two electrolytes. (**a** and **b**) P2p and (**c** and **d**) F1s XPS depth profiles of graphite electrode after 50 cycles with different electrolytes. (**a** and **c**) 1 M KFSI-FTEP electrolyte. (**b** and **d**) 1 M KFSI-TEP electrolyte. (**e**) The atomic ratios of P, F, and S elementals on graphite electrodes at different depths after 50 cycles. (**f**) The atomic ratios of S:P on graphite electrodes at different depths after 50 cycles.

Obviously, compared to the 1 M KFSI-TEP electrolyte, the graphite electrode with 1 M KFSI-FTEP electrolyte exhibits a lower P2p XPS peak intensity while a higher KF peak intensity of F1s XPS. These results indicating that the decomposition of TEP solvent is more severe than that of FTEP solvent, similar to the XPS results of 5 cycles.

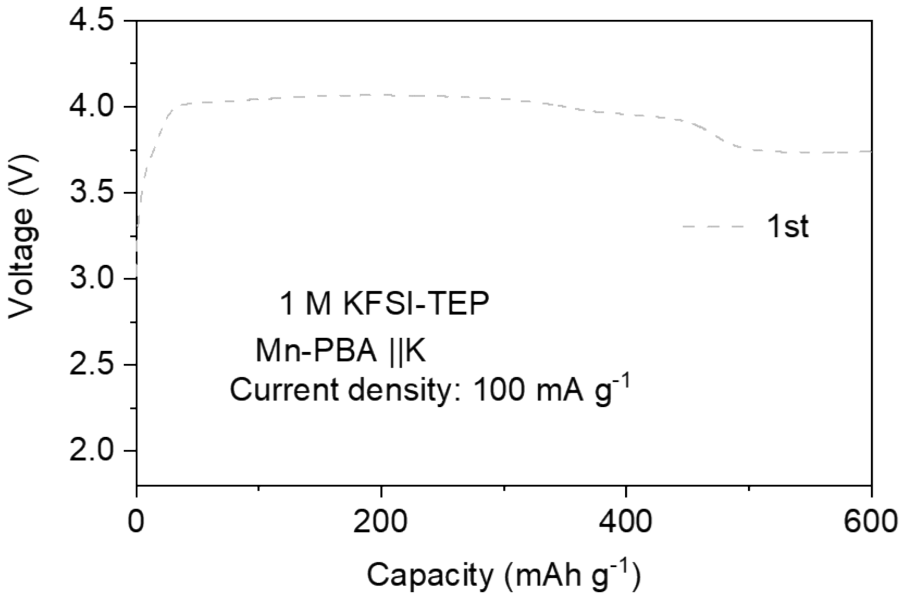

Fig. S19. The charge profile of Mn-PBA cathode with 1 M KFSI-TEP electrolyte.

Table S1. The ionic conductivities of various electrolytes.

Electrolytes	1 M KFSI-FTEP	1 M KFSI-TEP
Ionic conductivities	0.75 mS cm^{-1}	6.14 mS cm^{-1}

Table S2 The summary of graphite performance with various electrolytes.

Electrolytes	Running time (month)	Capacity retention	Reversible capacity	Rate performance	CE (%)
1 M KFSI-FTEP (**This work**)	26	~82.2% after 1732 cycles	241 mAh g^{-1} after 1732 cycles at 50 mA g^{-1}	291, 274, 216, 108, 77, 54 mAh g^{-1} at 50, 100 , 200 , 300, 400, 500 mA g^{-1}	~99.4
0.8 M KPF_6/EC-DEC[S1]	0.19	~50.8% after 50 cycles	100 mAh g^{-1} after 50 cycles at140 mA g^{-1}	263, 234, 172, 80 mAh g^{-1} at C/10, C/5 , C/2 , 1C	~ 99
1.0 m KFSI TMP +6 wt%DTD[S2]	0.75	~91.3% after 100 cycles	272 mAh g^{-1} after 100 cycles at 100 mA g^{-1}	277, 266, 254, 248, 241, 235 , 228 mAh g^{-1} at 0.2 , 0.4 , 0.8, 1.2, 1.6, 2, 2.4C	Not give
0.8 m KPF_6 EC/DEC[S3]	0.9	~76.9% after 250 cycles	~200 mAh g^{-1} after 250 cycles at 200 mA g^{-1}	391.8, 315.6, 286.1, 223.9, 156.9, 124.7, 76.1 mAh g^{-1} at 0.05, 0.1, 0.2, 0.5, 0.8, 1.0, 2.0 A g^{-1}	~95
1.5 M KFSI PC/TEG[S4]	1.7	~90.9% after 400 cycles	202 mAh g^{-1} after 400 cycles at 140 mA g^{-1}	~ 243, 230, ~224, ~206, 190 mAh g^{-1} at 0.025C, 0.1C, 0.2C, 0.5C, 1C	~99.9
1 mol KFSA EC:DEC[S5]	2	~82% after 100 cycles	202 mAh g^{-1} after 100 cycles at 28 mA g^{-1}	Not give	Not give
0.5 M KPF_6 EC/DEC +0.2 wt% KDFP[S6]	2.8	~77% after 400 cycles	181 mAh g^{-1} after 400 cycles at 93 mA g^{-1}	272, ~240, ~225, ~179, 60, 23 mAh g^{-1} at C/20, C/10, C/5, C/2, 1C, 2C	~99.9
1 M KPF_6 EC DME[S7]	6	~80% after 500 cycles	220 mAh g^{-1} after 500 cycles at 50 mA g^{-1}	Not give	~99

1 m KPF_6 EC/PC[S8]	6.1	~89.1% after 200 cycles	246 mAh g^{-1} after 200 cycles at 20 mA g^{-1}	253, 212, 156, 79, 11 mAh g^{-1} at 20, 50, 100, 200, 500 mA g^{-1}	~99.5
7 mol kg^{-1} KFSI DME[S9]	0.23	~85.3% after 50 cycles	232 mAh g^{-1} after 50 cycles at 140 mA g^{-1}	Not give	ICE: 80.8
2 M KFSI TEP[S10]	4.1	~90.2% after 300 cycles	248 mAh g^{-1} after 300 cycles at 55 mA g^{-1}	280, 270, 250, 200, 150, 45 and 275 mAh g^{-1} at 0.1C, 0.2C, 0.5C, 1C, 2C, 5C and 0.1C	99.7
7 mol kg^{-1} KFSA/DME[S11]	8.6	~92.7% after 300 cycles	~241 mAh g^{-1} after 300 cycles at 25 mA g^{-1}	282, ~278, ~274, ~261, 258, 253 mAh g^{-1} at C/10, C/5, C/2, 1C, 2C, 5C	Not give
KFSI:EMC= (1:2.5)[S12]	17	~99.2% after 2000 cycles	253 mAh g^{-1} after 2000 cycles at C/3 mA g^{-1}	Not give	99.9
KFSI:TMP = 3:8[S13]	24	~74.2% after 50 cycles	~230 mAh g^{-1} after 2000 cycles at 55 mA g^{-1}	~275, ~269, ~246, ~170, ~103, ~51 mAh g^{-1} at 0.1C, 0.2C, 0.5C, 1C, 2C, 5C	99.6

Table S3. The atomic contents of P and S elements obtained from the SEM EDS of Cu electrodes in different electrolytes.

Electrolytes/ Elements	1 M KFSI-FTEP after plating	1 M KFSI-TEP after plating	1 M KFSI-FTEP after stripping	1 M KFSI-TEP after stripping
P	0.13	4.04	0.15	1.56
S	0.80	3.60	1.21	1.59

Table S4. The atomic contents of P and S elements obtained from the SEM EDS of graphite electrodes in different electrolytes.

Electrolytes/ Elements	1 M KFSI-FTEP after 5 cycles	1 M KFSI-TEP after 5 cycles	1 M KFSI-FTEP after 50 cycles	1 M KFSI-TEP after 50 cycles
P	0.04	3.45	0.22	4.14
S	0.41	1.41	1.01	2.10

References

S1. Z. Jian, W. Luo and X. Ji, *J. Am. Chem. Soc.*, 2015, **137**, 11566-11569.

S2. G. Liu, Z. Cao, L. Zhou, J. Zhang, Q. J. Sun, J. Y. Hwang, L. Cavallo, L. M. Wang, Y. K. Sun and J. Ming, *Adv. Funct. Mater.*, 2020, **30**, 2001934.

S3. D. Wang, L. Li, Z. Zhang, J. Liu, X. Guo, C. Mao, H. Peng, Z. Li and G. Li, *Small*, 2021, **17**, e2103557.

S4. S. Q. Liu, L. C. Meyer, L. Medenbach and A. Balducci, *Energy Storage Mater.*, 2022, **47**, 534-541.

S5. M. Shimizu, T. Koya, A. Nakahigashi, N. Urakami, T. Yamakami and S. Arai, *J. Phys. Chem. C*, 2020, **124**, 13008-13016.

S6. H. Yang, C. Y. Chen, J. Hwang, K. Kubota, K. Matsumoto and R. Hagiwara, *ACS Appl. Mater. Interfaces*, 2020, **12**, 36168-36176.

S7. M. Gu, L. Fan, J. Zhou, A. M. Rao and B. Lu, *ACS Nano*, 2021, **15**, 9167-9175.

S8. J. Zhao, X. X. Zou, Y. J. Zhu, Y. H. Xu and C. S. Wang, *Adv. Funct. Mater.*, 2016, **26**, 8103-8110.

S9. X. B. Niu, L. Li, J. L. Qiu, J. Y. Yang, J. Huang, Z. R. Wu, J. Zou, C. Jiang, J. Gao and L. P. Wang, *Solid State Ionics*, 2019, **341**.

S10. S. Liu, J. Mao, Q. Zhang, Z. Wang, W. K. Pang, L. Zhang, A. Du, V. Sencadas, W. Zhang and Z. Guo, *Angew. Chem. Int. Ed.*, 2020, **59**, 3638-3644.

S11. T. Hosaka, K. Kubota, H. Kojima and S. Komaba, *Chem. Commun.*, 2018, **54**, 8387-8390.

S12. L. Fan, R. Ma, Q. Zhang, X. Jia and B. Lu, *Angew. Chem. Int. Ed.*, 2019, **58**, 10500-10505.

S13. S. Liu, J. Mao, L. Zhang, W. K. Pang, A. Du and Z. Guo, *Adv. Mater.*, 2021, **33**, e2006313.